run in TBE ×0.5 at room temperature for 2 h at 150 V. The following two (*Q*/*q*) 27-bp unmethylated oligonucleotides were used: 5′-GATCCTTCGCCTAGGCTC(A/G)CAGCG CGGGAGCGA-3′. A methylated *q* probe (*q**) was generated by incorporating a methylated cytosine at the mutated CpG site during oligonucleotide synthesis.

Transient transfection assay

The constructs contained 578 bp from *IGF2* intron 3 (nucleotides 2868–3446), followed by the *IGF2* P3 promoter (nucleotides −222 to +45 relative to the start of transcription)[12] and a luciferase reporter. C2C12 myoblast cells were grown to approximately 80% confluence. Cells were transiently co-transfected with the firefly luciferase reporter construct (4 μg) and a Renilla luciferase control vector (phRG-TK, Promega; 80 ng) using 10 μg Lipofectamine 2000 (Invitrogen). Cells were incubated for 25 h before lysis in 100 μl Triton lysis solution. Luciferase activities were measured using the Dual-Luciferase Reporter Assay System (Promega). The results are based on four triplicate experiments using two independent plasmid preparations for each construct. Statistical analysis was done with an analysis of variance.

Northern blot analysis and real-time RT–PCR

Total RNA was prepared using Trizol (Invitrogen) and treated with DNase I (Ambion). Products from the first-strand complementary DNA synthesis (Amersham Biosciences) were purified with QIAquick columns (Qiagen). Poly(A)$^+$ RNA was then isolated using the Oligotex mRNA kit (Qiagen). Poly(A)$^+$ mRNA (about 75 ng) from each sample was separated in a MOPS/formaldehyde agarose gel and transferred overnight to a Hybond-N$^+$ nylon membrane (Amersham Biosciences). The membrane was hybridized in ExpressHyb hybridization solution (Clontech). The quantification of the transcripts was performed with a Phosphor Imager 425 (Molecular Dynamics). Real-time PCR was performed with an ABI PRISM 7700 instrument (Applied Biosystems). TaqMan probes and primers are given in Supplementary Table 3. PCRs were performed in triplicate using the Universal PCR Master Mix (Applied Biosystems). Messenger RNA was quantified using ten-point calibration curves established by dilution series of the cloned PCR products. Statistical evaluations were done with a two-sided Kruskal–Wallis rank-sum test.

Received 11 June; accepted 11 September 2003; doi:10.1038/nature02064.

1. Mackay, T. F. C. Quantitative trait loci in *Drosophila*. *Nature Rev. Genet.* **2,** 11–21 (2001).
2. Andersson, L. Genetic dissection of phenotypic diversity in farm animals. *Nature Rev. Genet.* **2,** 130–138 (2001).
3. Glazier, A. M., Nadeau, J. H. & Aitman, T. J. Finding genes that underlie complex traits. *Science* **298,** 2345–2349 (2002).
4. Darvasi, A. & Pisante-Shalom, A. Complexities in the genetic dissection of quantitative trait loci. *Trends Genet.* **18,** 489–491 (2002).
5. Jeon, J.-T. *et al.* A paternally expressed QTL affecting skeletal and cardiac muscle mass in pigs maps to the *IGF2* locus. *Nature Genet.* **21,** 157–158 (1999).
6. Nezer, C. *et al.* An imprinted QTL with major effect on muscle mass and fat deposition maps to the IGF2 locus in pigs. *Nature Genet.* **21,** 155–156 (1999).
7. King, M. C. & Wilson, A. C. Evolution at two levels in humans and chimpanzees. *Science* **188,** 107–116 (1975).
8. Nezer, C. *et al.* Haplotype sharing refines the location of an imprinted QTL with major effect on muscle mass to a 250 Kb chromosome segment containing the porcine *IGF2* gene. *Genetics* **165,** 277–285 (2003).
9. Florini, J. R., Ewton, D. Z. & McWade, F. J. IGFs, muscle growth, and myogenesis. *Diabetes Rev.* **3,** 73–92 (1995).
10. Evans, G. J. *et al.* Identification of quantitative trait loci for production traits in commercial pig populations. *Genetics* **164,** 621–627 (2003).
11. de Koning, D. J. *et al.* Genome-wide scan for body composition in pigs reveals important role of imprinting. *Proc. Natl Acad. Sci. USA* **97,** 7947–7950 (2000).
12. Amarger, V. *et al.* Comparative sequence analysis of the *Insulin-IGF2–H19* gene cluster in pigs. *Mamm. Genome* **13,** 388–398 (2002).
13. Greally, J. M., Guinness, M. E., McGrath, J. & Zemel, S. Matrix-attachment regions in the mouse chromosome 7F imprinted domain. *Mamm. Genome* **8,** 805–810 (1997).
14. Constancia, M. *et al.* Deletion of a silencer element in Igf2 results in loss of imprinting independent of H19. *Nature Genet.* **26,** 203–206 (2000).
15. Eden, S. *et al.* An upstream repressor element plays a role in Igf2 imprinting. *EMBO J.* **20,** 3518–3525 (2001).
16. Giuffra, E. *et al.* The origin of the domestic pig: independent domestication and subsequent introgression. *Genetics* **154,** 1785–1791 (2000).
17. Grobet, L. *et al.* A deletion in the bovine myostatin gene causes the double-muscled phenotype in cattle. *Nature Genet.* **17,** 71–74 (1997).
18. Milan, D. *et al.* A mutation in *PRKAG3* associated with excess glycogen content in pig skeletal muscle. *Science* **288,** 1248–1251 (2000).
19. Galloway, S. M. *et al.* Mutations in an oocyte-derived growth factor gene (BMP15) cause increased ovulation rate and infertility in a dosage-sensitive manner. *Nature Genet.* **25,** 279–283 (2000).
20. Mulsant, P. *et al.* Mutation in bone morphogenetic protein receptor-IB is associated with increased ovulation rate in Booroola Merino ewes. *Proc. Natl Acad. Sci. USA* **98,** 5104–5109 (2001).
21. Pailhoux, E. *et al.* A 11.7-kb deletion triggers intersexuality and polledness in goats. *Nature Genet.* **29,** 453–458 (2001).
22. Freking, B. A. *et al.* Identification of the single base change causing the callipyge muscle hypertrophy phenotype, the only known example of polar overdominance in mammals. *Genome Res.* **12,** 1496–1506 (2002).
23. Grisart, B. *et al.* Positional candidate cloning of a QTL in dairy cattle: identification of a missense mutation in the bovine *DGAT1* gene with major effect on milk yield and composition. *Genome Res.* **12,** 222–231 (2002).
24. Haley, C. S., Knott, S. A. & Elsen, J. M. Mapping quantitative trait loci in crosses between outbred lines using least squares. *Genetics* **136,** 1195–1207 (1994).
25. Anderson, S. I., Lopez-Corrales, N. L., Gorick, B. & Archibald, A. L. A large fragment porcine genomic library resource in a BAC vector. *Mamm. Genome* **11,** 811–814 (2000).
26. Nickerson, D., Tobe, V. O. & Taylor, S. L. PolyPhred: automating the detection and genotyping of single nucleotide substitutions using fluorescent-based resequencing. *Nucleic Acids Res.* **25,** 2745–2751 (1997).
27. Engemann, S., El-Maarri, O., Hajkova, P., Oswald, J. & Walter, J. in *Methods in Molecular Biology* Vol. 181 (ed. Ward, A.) (Humana Press, Totowa, New Jersey, 2002).
28. Andrews, N. C. & Faller, D. V. A rapid micropreparation technique for extraction of DNA-binding proteins from limiting numbers of mammalian cells. *Nucleic Acids Res.* **19,** 2499 (1991).
29. Kashuk, C., Sengupta, S., Eichler, E. & Chakravarti, A. ViewGene: a graphical tool for polymorphism visualization and characterization. *Genome Res.* **12,** 333–338 (2002).

Supplementary Information accompanies the paper on **www.nature.com/nature**.

Acknowledgements We thank C. Charlier and H. Ronne for discussions, M. Laita, B. McTeir, J. Pettersson, A.-C. Svensson and M. Köping-Höggård for technical assistance, and the Pig Improvement Company for providing DNA samples from Berkshire and Gloucester Old Spot pigs. This work was supported by the Belgian Ministère des Classes Moyennes et de l'Agriculture, the AgriFunGen program at the Swedish University of Agricultural Sciences, the Swedish Research Council for Environment, Agricultural Sciences and Spatial Planning, Gentec, the UK Department for Environment, Food and Rural Affairs, the UK Pig Breeders Consortium, and the Biotechnology and Biological Sciences Research Council.

Competing interests statement The authors declare competing financial interests: details accompany the paper on **www.nature.com/nature**.

Correspondence and requests for materials should be addressed to L.A. (Leif.Andersson@imbim.uu.se) or M.G. (michel.georges@ulg.ac.be). The sequence data reported in this paper have been deposited in GenBank under accession numbers AY242098–AY242112.

Identification of the haematopoietic stem cell niche and control of the niche size

Jiwang Zhang[1], Chao Niu[1], Ling Ye[2], Haiyang Huang[2], Xi He[1], Wei-Gang Tong[1], Jason Ross[1], Jeff Haug[1], Teri Johnson[1], Jian Q. Feng[2], Stephen Harris[2], Leanne M. Wiedemann[1,4], Yuji Mishina[3] & Linheng Li[1,4]

[1]*Stowers Institute for Medical Research, Kansas City, Missouri 64110, USA*
[2]*Department of Oral Biology, School of Dentistry, University of Missouri–Kansas City, 650 East 25th Street, Kansas City, Missouri 64108, USA*
[3]*Laboratory of Reproductive and Developmental Toxicology, National Institute of Environmental Health Sciences, Research Triangle Park, North Carolina 27709, USA*
[4]*Department of Pathology and Laboratory Medicine, Kansas University Medical Center, Kansas City, Kansas 66160, USA*

Haematopoietic stem cells (HSCs) are a subset of bone marrow cells that are capable of self-renewal and of forming all types of blood cells (multi-potential)[1]. However, the HSC 'niche'—the *in vivo* regulatory microenvironment where HSCs reside—and the mechanisms involved in controlling the number of adult HSCs remain largely unknown. The bone morphogenetic protein (BMP) signal has an essential role in inducing haematopoietic tissue during embryogenesis[2,3]. We investigated the roles of the BMP signalling pathway in regulating adult HSC development *in vivo* by analysing mutant mice with conditional inactivation of BMP receptor type IA (BMPRIA). Here we show that an increase in the number of spindle-shaped N-cadherin$^+$CD45$^-$ osteoblastic (SNO) cells correlates with an increase in the number of HSCs. The long-term HSCs are found attached to SNO cells. Two adherens junction molecules, N-cadherin and β-catenin, are asymmetrically localized between the SNO cells and the long-term HSCs. We conclude that SNO cells lining the bone surface function as a key component of the niche to support HSCs, and that BMP signalling through BMPRIA controls the number of HSCs by regulating niche size.

We first analysed the expression patterns of *Bmpr1a* (*Alk3*) and *Bmpr1b* (*Alk6*) in bone marrow and the surrounding bone tissue. BMPRIA was found in bone marrow cells, including most of the haematopoietic lineages apart from the HSC population, and most osteoblastic cells (Fig. 1a–c). By contrast, we were unable to detect expression of *Bmpr1b* in HSCs and the other haematopoietic lineages that we examined (Fig. 1d).

To block the BMP signal, we inactivated BMPRIA by crossing $Bmpr1a^{fx/fx}$ and $Bmpr1a^{fx/-}$ mouse lines[4] with a PolyI:C-inducible *Mx1–Cre* mouse line[5] and assaying the mutant mice. Multiple injections of PolyI:C were required for efficient deletion of *Bmpr1a* (see Supplementary Information, data 1)

Mice with different injection schedules (see Methods) were investigated using flow cytometric assays to analyse the HSC population. The percentage of lineage-negative (Lin^-) Sca-1^+c-Kit^+ (HSC) cells was increased 2-fold in the $Mx1–Cre^+Bmpr1a^{fx/fx}$ and 2.4-fold in the $Mx1–Cre^+Bmpr1a^{fx/-}$ mutant mice compared with the littermate controls (Fig. 2a). Although the total bone marrow cell number per femur was reduced in both of the *Bmpr1a* mutant lines owing to reduced cavity room, as seen in Fig. 3b, the absolute number of HSCs per femur was still increased 1.5–2-fold (Fig. 2b). As no significant difference between $Mx1–Cre^+Bmpr1a^{fx/fx}$ and $Mx1–Cre^+Bmpr1a^{fx/-}$ mutant mice was observed, we focused on the $Mx1–Cre^+Bmpr1a^{fx/fx}$ mice in the following studies.

The HSC population is a heterogeneous mixture, including long-term (LT) and short-term (ST) HSCs[6]. Therefore, we injected the mice with 5-bromodeoxyuridine (BrdU) to label cycling cells. Three hours after labelling, we analysed the HSC population to distinguish ST-HSCs from LT-HSCs according to differences in their cell-cycle state. The percentage of BrdU-negative cells in the HSC population (including the quiescent LT-HSCs) increased by an average of 2.4 times in the *Bmpr1a* mutant mice compared with littermate controls. The percentage of BrdU-positive cells in the HSC population

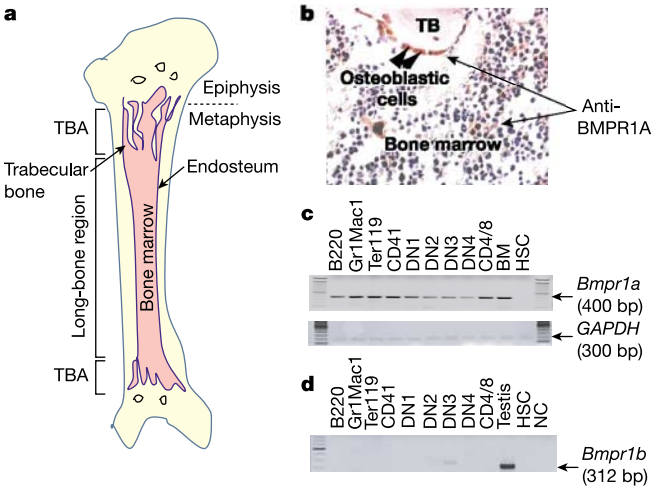

Figure 1 Expression patterns of BMPRIA and BMPRIB in bone and bone marrow. **a**, Schematic of bone and bone marrow structures. TBA, trabecular bone area. **b**, Expression of BMPRIA in osteoblastic cells and bone marrow cells. Bone/bone marrow sections were immunohistochemically stained using anti-BMPRIA serum. TB, trabecular bone. **c**, Detection of *Bmpr1a* gene expression in HSCs and lineage cells by RT–PCR (polymerase chain reaction with reverse transcription) assay. GAPDH, glyceraldehyde-3-phosphate; B220, B-cell marker; Gr1Mac1, myeloid lineage markers; Ter119, erythroid lineage marker; CD41, megakaryocyte marker; DN, double negative for CD4 and CD8; DN1, $CD44^+CD25^-$; DN2, $CD44^+CD25^+$; DN3, $CD44^-CD25^+$; DN4, $CD44^-CD25^-$. **d**, Detection of *Bmpr1b* gene expression in HSCs and lineage cells by RT–PCR assay. NC, negative control.

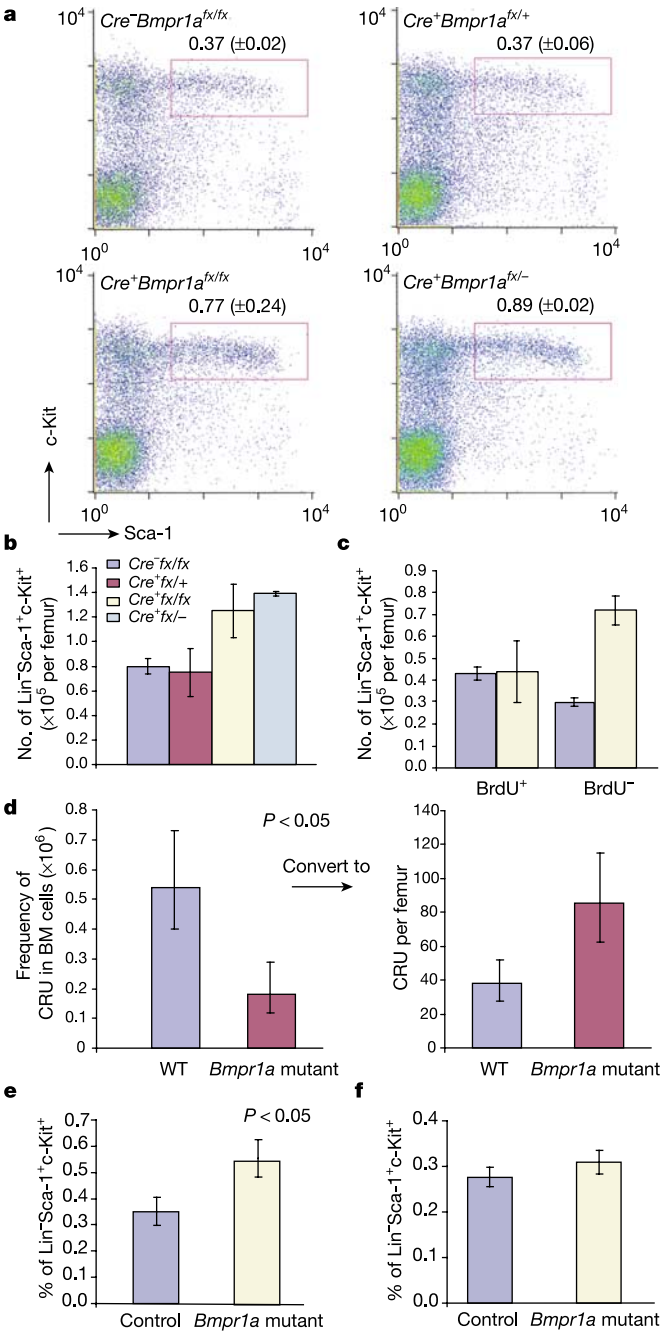

Figure 2 Analyses of the HSC population. For raw data, see Supplementary Tables 1–4. **a**, Typical example of flow assay on the HSC population. Figure in the gate is the percentage of HSCs in the BM-MNC fraction. **b**, Comparison of absolute number of HSCs per femur in wild-type and *Bmpr1a* mutant mice. Owing to the reduced bone cavity in *Bmpr1a* mutant mice, the total bone marrow cell number is also reduced in mutant mice (an average of 1.58×10^7 versus 2.1×10^7 in wild-type control mice). The absolute HSC number is equal to the percentage of HSCs multiplied by the total number of BM-MNCs. **c**, Comparison of the number of LT-HSCs and ST-HSCs in the *Bmpr1a* mutant and control mice. **d**, CRU assay to compare the number of functional HSCs per femur between the *Bmpr1a* mutant and wild-type (WT) control mice. The number of CRUs per femur (right panel) equals the frequency of CRUs (left panel) multiplied by the total number of BM-MNCs as indicated in **b**. **e**–**f**, Bar graphs of the percentage of HSCs in recipient mice. Wild-type donor (Ly5.1) HSCs (2×10^3) were transplanted into *Bmpr1a* mutant recipients or littermate controls (Ly5.2) (**e**). Bone marrow cells (2×10^6) from controls and mutants (Ly5.2) were transplanted into wild-type recipients (Ly5.1) (**f**).

(including the cycling ST-HSCs) was similar to that in the littermate controls (Fig. 2c). Therefore, direct comparison of the entire HSC population provides an underestimated but reliable representation (Fig. 2b; 1.6-fold) of the difference in LT-HSC numbers (Fig. 2c; 2.4-fold) between the mutant and control animals.

These experiments demonstrated an increase in the LT-HSC population. However, the gold-standard test for functional stem cells is the competitive repopulation unit (CRU) assay[7], in which a series of diluted donor-derived bone marrow mononuclear cells (BM-MNCs) is transplanted into different groups of sublethally irradiated recipient mice. Three months after transplantation, peripheral blood is examined to monitor the engraftment of donor cells in the recipient mice in order to determine the lowest number of bone marrow cells required for the reconstitution of haematopoiesis. Using this assay, we confirmed that the functional stem cell number increased 2.2-fold in the mutant mice compared with controls (Fig. 2d and Supplementary Table 4). The results from both immunophenotypical and CRU assays indicate that the population of LT-HSCs is expanded in the *Bmpr1a* mutant mice.

There are several mechanisms that can lead to changes in the HSC number: (1) an intrinsic change in stem cells that either promotes self-renewal or blocks apoptosis; (2) an internal defect in progenitors that inhibits differentiation, leading to an accumulation of stem cells; or (3) an external influence from the HSC microenvironment. The finding that *Bmpr1a* is not expressed in HSCs (Fig. 1c) does not support the argument that an intrinsic defect in HSCs was the cause of a change in the number of HSCs in the *Bmpr1a* mutant mice. We then analysed myeloid and lymphoid lineages, common myeloid progenitor and common lymphoid progenitor subsets[8,9]. The results revealed no significant phenotypical change in any of the subsets analysed (Supplementary Information, data 2a, b). This was consistent with results obtained from *in vitro* colony-forming unit

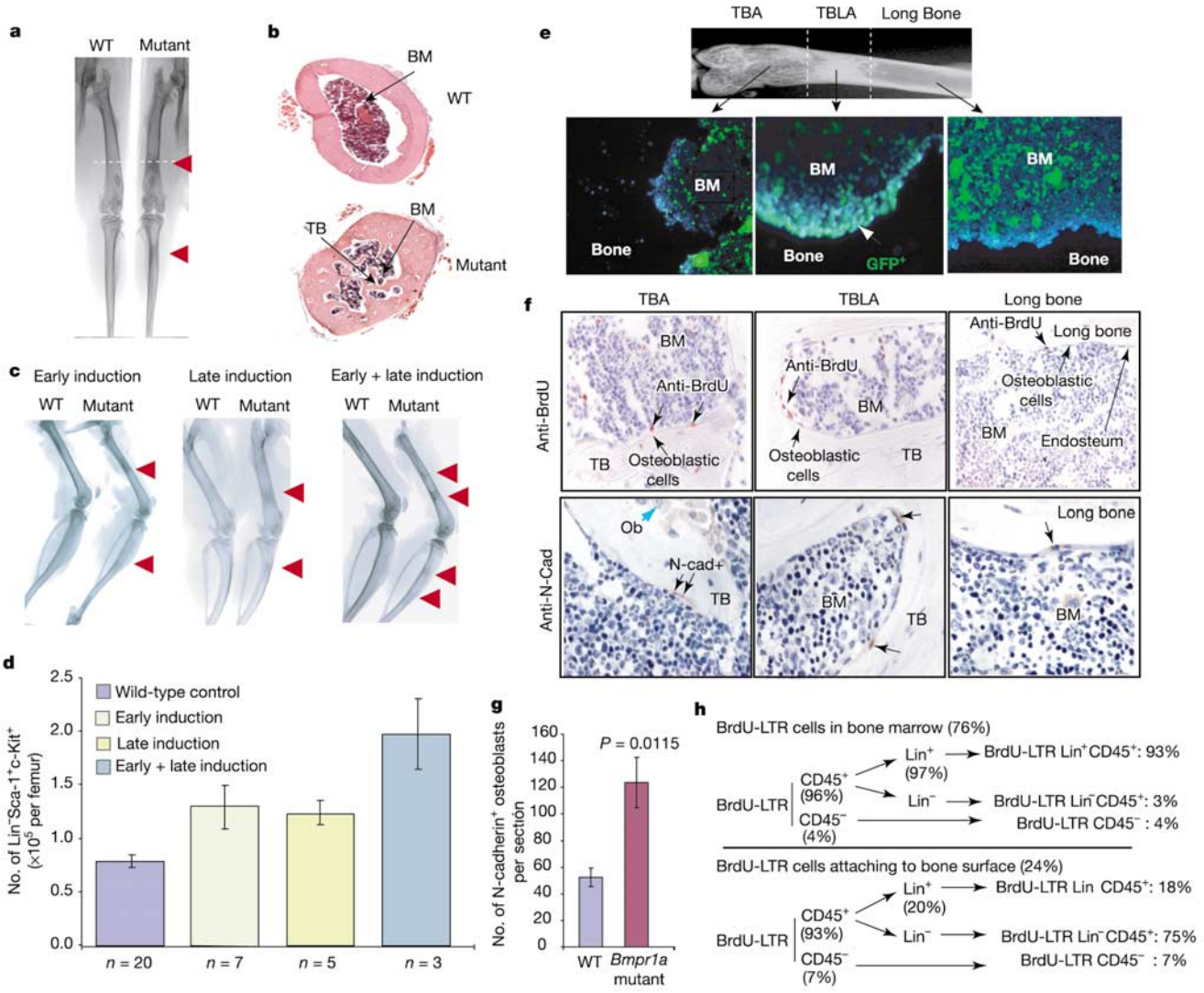

Figure 3 Analyses of bone structure and HSC number. **a**, **b**, X-ray image and histology of the bone structures of ectopically formed TBLA (red arrow). BM, bone marrow. **c**, X-ray images of femur and tibia from *Bmpr1a* mutant and control mice. **d**, Comparison of the absolute number of HSCs per femur in *Bmpr1a* mutant and wild-type control mice. **e**, Inactivation of *Bmpr1a* on the surface of ectopically formed TBLA in the triple-genotype mice as shown by GFP expression, counterstained with 4,6-diamidino-2-phenylindole (DAPI). **f**, BrdU-LTR cells (upper panels, black arrow), SNO cells (lower panels, black arrow) and matrix-forming osteoblasts (blue arrow). **g**, SNO cell number in control and *Bmpr1a* mutant mice. (The average total number of the SNO cells per section is given in Supplementary Table 6.) **h**, Summary of the distribution of three types of BrdU-LTR cell (see text and Supplementary Table 7).

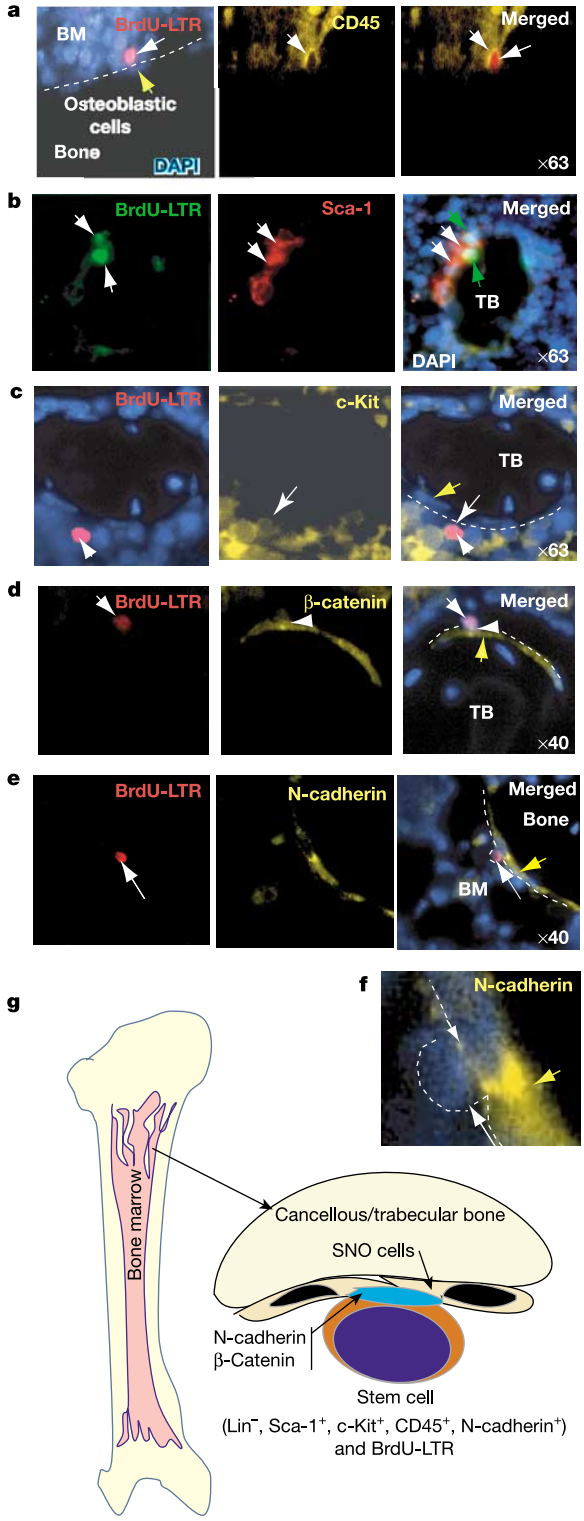

Figure 4 Co-staining of BrdU-LTR cells with HSC markers, counterstained with DAPI. **a**–**e**, HSC markers as indicated. The lens magnification used for the microscopic photograph is indicated. Most BrdU-LTR cells attached to the trabecular bone surface are co-stained with Sca-1 (74%), c-Kit (72%) or a pan-haematopoietic marker, CD45 (92%). Yellow arrow indicates SNO cells. **f**, A blow-up of part **e**. **g**, Model illustrating the haematopoietic stem cell niche. The SNO cells, which are located mainly on the surface of cancellous/trabecular bone, are a key component of the resident niche for HSCs.

(CFU) assays, which showed that the progenitor number of different lineages was similar in the *Bmpr1a* mutant and littermate control mice (Supplementary Information, data 3). These results ruled out the possibility of an accumulation of HSCs resulting from a block in progenitor cell differentiation.

Direct evidence of an external influence causing the change in HSC number came from reciprocal bone marrow/HSC transplantation experiments. HSCs isolated from wild-type Ly5.1 mice were transplanted into lethally irradiated *Bmpr1a* mutant and littermate control mice (both Ly5.2 genotype). The result of a flow cytometric assay three months after transplantation revealed that the percentage of donor-derived HSCs in the *Bmpr1a* mutant mice was, on average, 1.6 times higher than in the wild-type control recipient mice (Fig. 2e). A reciprocal assay was also carried out by transplanting BM-MNCs derived from the *Bmpr1a* mutant or wild-type control mice into lethally irradiated wild-type Ly5.1 mice. These flow cytometric results showed that the percentage of donor-derived HSCs in both groups of recipient mice was similar, regardless of the origin of BM-MNCs (Fig. 2f). We conclude that the change in the microenvironment led to an increase in HSC number in the *Bmpr1a* mutant mice.

Bone marrow stromal cells are derived from mesenchymal stem cells, including fibroblasts, adipocytes, endothelial cells and osteoblasts[10]. Previous studies of the roles of stromal cells in supporting HSCs have been based mainly on *in vitro* culture, and each of these stromal cells has been suggested to be capable of supporting haematopoietic stem/progenitor cells *in vitro*[11,12]. However, none of these results has been confirmed *in vivo*.

We observed obvious abnormal bone formation in the *Bmpr1a* mutant mice. Our X-ray and histological analyses revealed that an ectopic formation of trabecular-bone-like area (TBLA) occurred in the long-bone region of the mutant mice (Fig. 3a, b). The location of the ectopically formed TBLAs varied depending on the PolyI:C injection time: TBLAs were seen distal to the knee in the early-induced group, but were proximal to the knee in the late-induced group, and at both sites in the combined-injection group (Fig. 3c). This raised the possibility of a change in osteoblasts or osteoclasts affecting the HSC microenvironment. Recent *in vitro* evidence shows that an osteoblastic cell line can expand the number of HSCs 2–4-fold[12]. In addition, osteoblasts, when co-transplanted with HSCs, can also increase the engraftment rate[13]. These observations suggest that osteoblasts have a role in supporting HSCs.

We next asked whether the ectopically formed TBLA was responsible for the increased HSC number in the mutant mice. As described above (Fig. 2b), the number of HSCs per femur in the mutant animals was increased 1.67-fold on average in both early- and late-induced mutant mice. In addition, we found that the number of HSCs per femur increased 2.5-fold on average in the combined early- and late-induced mice, in which two regions of TBLA were observed (Fig. 3d). This shows that an increase in the number of HSCs correlates with an increase in the number of ectopically formed TBLAs.

We investigated the mechanism that leads to the ectopic formation of TBLA when the BMP signal is blocked. BMPRIA has been shown to inhibit osteoblastic lineage commitment from mesenchymal progenitors *in vitro*[14]. We ruled out the possibility of an increase in the number of mesenchymal progenitors in the mutants using a CFU-fibroblast assay[10] (Supplementary Table 5). Osteoblastic lineage commitment from mesenchymal progenitors is not increased, because the ectopic formation of TBLA is regional rather than evenly distributed. This suggests that regional inactivation of *Bmpr1a* leads to the ectopic formation of TBLA. To confirm this, we generated a triple-genotype mouse line bearing *Mx1–Cre*, $Bmpr1a^{fx/fx}$ and *Z/EG* alleles. Cre-induced green fluorescent protein (GFP) expression reflects successful targeting of *Bmpr1a* (Fig. 3e). Analysis of bone sections derived from the triple-genotype mice revealed that only the surface of ectopically formed TBLA was GFP

positive, indicating that regional deletion of *Bmpr1a* occurs exclusively in the cells that line the TBLA surface. This was further supported by a 3-fold increase in osteoblast number, a 2-fold increase in the rate of bone formation, and a 10-fold increase in bone volume in the TBLA of *Bmpr1a* mutants compared with the long-bone region in control littermates (Supplementary Information, data 4, and Supplementary Table 8); however, there was no apparent change in osteoclasts (cells that reabsorb bone) measured by tartrate-resistant acid phosphatase staining (data not shown). The ectopic TBLA might be formed by over-proliferation or abnormal differentiation of an osteoblast progenitor. In addition, inactivation of BMPRIA might make the osteoblasts less sensitive to apoptotic signal, as a BMP signal is known to induce osteoblast apoptosis[15].

We observed a correlation between the number of LT-HSCs and the increase in TBLA. Are the LT-HSCs in the TBLA enriched? The limited number of LT-HSCs in bone marrow and the lack of a unique marker make their visualization difficult. As LT-HSCs are quiescent or slow cycling, they are able to retain labelled nucleotides for a relatively long period and can be identified as BrdU-LTR (long-term retaining) cells[16] (see Methods). We found that 76% of the BrdU-LTR cells were located within the bone marrow cavity, whereas 24% were attached to the bone surface. Most BrdU-LTR cells attached to the bone surface were located in cancellous/trabecular bone area (including epiphysis and metaphysis), whereas the rest were dispersed along the endosteal surface of long bone (Fig. 3f, upper panel). This is consistent with previous observations in which HSCs were found to be close to the endosteal surface of long bone[17] or homing to the bone surface of epiphysis[18]. Importantly, a significantly increased number of BrdU-LTR cells was found in the ectopically formed TBLA compared with the long-bone region (Fig. 3f). There are different types of BrdU-LTR cell, including Lin^-CD45^+ (enriched with LT-HSCs), Lin^+CD45^+ (enriched with memory T or B cells) and Lin^-CD45^- (enriched with mesenchymal stem cells) (see Fig. 3h). We estimate that the frequency of the enriched LT-HSCs in control animals (BrdU-LTR Lin^-CD45^+ cells) is 0.01%, close to the frequency of LT-HSCs (0.007%) on the basis of functional studies[19]. These cells are located mainly on the bone surface, particularly the surface of the cancellous/trabecular bone, and most of these cells are co-stained with other HSC markers: CD45, Sca-1 and c-Kit (Fig. 4a–c). These observations support the conclusion that the ectopically formed TBLA is responsible for the increase in the number of HSCs.

The increased number of osteoblasts on the surface of ectopically formed TBLA correlates with the increase in HSC number. The LT-HSCs appear to be attached to cells with an early osteoblastic character (the mononuclear spindle-shaped cells lining the bone surface; Fig. 3f, upper panel). As N-cadherin is expressed in both early and late osteoblastic cells[20], we used this biological marker to confirm this observation. This marker stains two osteoblastic cell types: a small subset of spindle-shaped osteoblasts (osteoblastic lining cells) and most of the larger, oval-shaped, matrix-forming osteoblasts (Fig. 3f, lower panel). Histological analysis of the distribution of the spindle-shaped N-cadherin$^+$ osteoblastic (SNO) cells revealed that these cells were enriched on the surface of cancellous/trabecular bone, including the vesicle area in epiphysis, and sporadically dispersed along the endosteal surface of long bone (Fig. 3f, lower panel). This distribution pattern was similar to that of LT-HSCs (Fig. 3f, upper panel). Indeed, the LT-HSCs are attached only to the SNO cells that line the bone surface, (Fig. 4e). We also counted the number of SNO cells (Supplementary Table 6). The result showed that an increase in the number of these cells (2.3-fold; Fig. 3g) correlates to a high degree with the increase in LT-HSC number (2.2-fold; Fig. 2d) in the *Bmpr1a* mutant mice. Taken together, these observations indicate that the SNO cells have an important role in supporting LT-HSCs. This conclusion is also supported by evidence from studies of conditional ablation of osteoblasts in Col2.3Δtk (thymidine kinase) transgenic mice, which showed that osteoblasts were necessary for the maintenance of haematopoiesis and where a loss of osteoblasts led to loss of haematopoietic cells[21].

As the functions of the niche include adhesive interaction between stem cells and the niche[22], we asked whether the SNO cells provide an adhesive attachment for HSCs. In *Drosophila*, two important junction-related adherens molecules, E-cadherin and β-catenin, are essential for the maintenance of ovarian somatic stem cells, as evidenced by the observation that a loss of E-cadherin leads to a loss of somatic stem cells[23]. E-cadherin was not expressed in either the osteoblasts or the LT-HSCs (although it was expressed in many bone marrow cells; data not shown). However, we found that N-cadherin was asymmetrically localized to the cell surface of LT-HSCs adjacent to the SNO cells (Fig. 4e, f). Using flow cytometric assay, we confirmed that N-cadherin is expressed in a subpopulation (10%) of murine adult HSCs ($Lin^-Sca\text{-}1^+c\text{-}Kit^+$) (Supplementary Information, data 5). It will be important to demonstrate an *in vivo* functional role of the N-cadherin$^+$ HSCs. In addition, β-catenin, which interacts with and forms an adherens complex with N-cadherin[24], is also found to be asymmetrically localized between the SNO cells and the LT-HSCs (Fig. 4d).

The niche hypothesis was first proposed by Schofield[25] in 1978, and is supported by the co-culture of HSCs with marrow stromal cells[26]. The stem cell niche has been described in the *Drosophila* ovary[27], but the HSC niche, owing to complicated anatomical architecture, has remained an enigma. We show that, in bone and bone marrow, the cancellous/trabecular bone area is the primary site for HSCs. The SNO cells located on the bone surface are a key component of the niche, supporting LT-HSCs (Fig. 4g). SNO cells might support HSCs through a specific adhesive interaction between N-cadherin and β-catenin. Consistent with this, in col1-PPR (parathyroid hormone (PTH)/PTHrP receptor) transgenic mice, the osteoblastic lineage has been defined as a key participant in the regulation of HSC numbers[28]. The niche size must be tightly regulated *in vivo* to maintain HSCs and normal homeostasis[25,29]. We provide *in vivo* evidence to show that a change in the niche size affects the number of stem cells. BMP signalling through BMPRIA is an important component of this regulatory system. □

Methods

Inducible Cre expression

PolyI:C (250 μg per mouse) was injected intraperitoneally. For the early-induced group, PolyI:C was injected on the 3rd, 5th and 7th day after birth, whereas the late-induced group was treated with PolyI:C on the 21st, 23rd and 25th day after birth. A third double-induced group combined both injection schedules.

Flow cytometric assay and CFU culture

Isolation and preparation of bone marrow, thymus, spleen and peripheral blood cells, and the method for subsequent flow cytometric assays have been described[30]. For HSC analysis, BM-MNCs were stained with fluorescein isothiocyanate (FITC)-lineage markers (CD4, CD8, CD3, B220, IgM, Mac-1, Gr-1 and Ter-119) to eliminate Lin^+ cells, but positive for APC-c-Kit and phycoerythrin (PE)-Sca-1. For lineage analyses, see Supplementary Information, data 1a, b. CFU assay was performed according to the manufacturer's recommendations (StemCell Technologies).

CRU assay

A series of diluted BM-MNCs (1×10^4, 3×10^4, 1×10^5 and 3×10^5) from either *Bmpr1a* mutant or wild-type control were transplanted into several groups of sublethally (500 rad) irradiated Ly5.1 recipient female mice. Three months after transplantation, peripheral blood was analysed using myeloid and lymphoid lineage markers: Mac-1, Gr-1, B220, CD3 and Ly5.2. An engraftment rate of >1% (the basal level was defined by transplantation of bone marrow derived from Ly5.1 mice) was scored as positive. The data shown in Fig. 2f are based on two independent experiments. The CRU frequencies were determined using L-Calc software (StemCell Technologies), which uses Poisson statistics and the method of maximum likelihood to the proportion of negative recipients, using limiting-dilution analysis (see Supplementary Table 4). We found that the CRU frequency was lower than that reported in studies where lethal doses of irradiation have been used[7].

Immunohistochemistry and BrdU-LTR assay

The procedures for bone and bone marrow section preparation, immunostaining conditions and antibodies are described in Supplementary Methods. The procedure for BrdU pulse labeling, LTR and subsequent detection has been reported[16]. The mice were fed BrdU (0.8 mg ml^{-1} in water) for 10 days, during which time 40% of LT-HSCs would divide at least once[31]. Seventy days after BrdU labelling, sections were stained with anti-BrdU antibody.

N-cadherin$^+$ cell count

For quantitative analysis of N-cadherin$^+$ cells, the sections were developed with AEC after being incubated with rabbit anti-N-cadherin antibody for 1 h and horseradish peroxidase (HRP)-conjugated goat anti-rabbit second antibody for 1 h. Three people counted the SNO cells in these sections, blind to the source of the sections.

X-ray image

High-resolution X-rays (Faxitron MX-20) of bone and bone histomorphometry (OsteoMetrics, Inc.) were performed at the University of Missouri–Kansas City School of Dentistry.

Received 12 May; accepted 12 August 2003; doi:10.1038/nature02041.

1. Spangrude, G. J., Heimfeld, S. & Weissman, I. L. Purification and characterization of mouse hematopoietic stem cells. *Science* **241,** 58–62 (1988).
2. Maeno, M. *et al.* The role of BMP-4 and GATA-2 in the induction and differentiation of hematopoietic mesoderm in *Xenopus laevis*. *Blood* **88,** 1965–1972 (1996).
3. Davidson, A. J. & Zon, L. I. Turning mesoderm into blood: the formation of hematopoietic stem cells during embryogenesis. *Curr. Top. Dev. Biol.* **50,** 45–60 (2000).
4. Mishina, Y., Hanks, M. C., Miura, S., Tallquist, M. D. & Behringer, R. R. Generation of Bmpr/Alk3 conditional knockout mice. *Genesis* **32,** 69–72 (2002).
5. Kuhn, R., Schwenk, F., Aguet, M. & Rajewsky, K. Inducible gene targeting in mice. *Science* **269,** 1427–1429 (1995).
6. Morrison, S. J. & Weissman, I. L. The long-term repopulating subset of hematopoietic stem cells is deterministic and isolatable by phenotype. *Immunity* **1,** 661–673 (1994).
7. Szilvassy, S., Nicolini, F. E., Eaves, C. J. & Miller, C. L. in *Hematopoietic Stem Cell Protocols* (eds Klug, C. A. & Jordan, C. T.) 167–187 (Humana Press, Totowa, New Jersey, 2002).
8. Kondo, M., Weissman, I. L. & Akashi, K. Identification of clonogenic common lymphoid progenitors in mouse bone marrow. *Cell* **91,** 661–672 (1997).
9. Akashi, K., Traver, D., Miyamoto, T. & Weissman, I. L. A clonogenic common myeloid progenitor that gives rise to all myeloid lineages. *Nature* **404,** 193–197 (2000).
10. Simmons, P., Gronthos, S. & Zannettino, A. C. in *Hematopoiesis: A Developmental Approach* (ed. Zon, L. I.) 718–726 (Oxford Univ. Press, New York, 2001).
11. Charbord, P. The hematopoietic stem cell and the stromal microenvironment. *Therapie* **56,** 383–384 (2001).
12. Taichman, R. S., Reilly, M. J. & Emerson, S. G. The hematopoietic microenvironment: osteoblasts and the hematopoietic microenvironment. *Hematology* **4,** 421–426 (2000).
13. El-Badri, N. S., Wang, B. Y. & Cherry Good, R. A. Osteoblasts promote engraftment of allogeneic hematopoietic stem cells. *Exp. Hematol.* **26,** 110–116 (1998).
14. Chen, D. *et al.* Differential roles for bone morphogenetic protein (BMP) receptor type IB and IA in differentiation and specification of mesenchymal precursor cells to osteoblast and adipocyte lineages. *J. Cell Biol.* **142,** 295–305 (1998).
15. Hay, E., Lemonnier, J., Fromigue, O. & Marie, P. J. Bone morphogenetic protein-2 promotes osteoblast apoptosis through a Smad-independent, protein kinase C-dependent signaling pathway. *J. Biol. Chem.* **276,** 29028–29036 (2001).
16. Taylor, G., Lehrer, M. S., Jensen, P. J., Sun, T. T. & Lavker, R. M. Involvement of follicular stem cells in forming not only the follicle but also the epidermis. *Cell* **102,** 451–461 (2000).
17. Nilsson, S. K., Johnston, H. M. & Coverdale, J. A. Spatial localization of transplanted hemopoietic stem cells: inferences for the localization of stem cell niches. *Blood* **97,** 2293–2299 (2001).
18. Askenasy, N. & Farkas, D. L. Optical imaging of PKH-labeled hematopoietic cells in recipient bone marrow *in vivo*. *Stem Cells* **20,** 501–513 (2002).
19. Lagasse, E., Shizuru, J. A., Uchida, N., Tsukamoto, A. & Weissman, I. L. Toward regenerative medicine. *Immunity* **14,** 425–436 (2001).
20. Hay, E. *et al.* N- and E-cadherin mediate early human calvaria osteoblast differentiation promoted by bone morphogenetic protein-2. *J. Cell. Physiol.* **183,** 117–128 (2000).
21. Visnjic, D. *et al.* Conditional ablation of the osteoblast lineage in Col2.3Δtk transgenic mice. *J. Bone Miner. Res.* **16,** 2222–2231 (2001).
22. Spradling, A., Drummond-Barbosa, D. & Kai, T. Stem cells find their niche. *Nature* **414,** 98–104 (2001).
23. Song, X. & Xie, T. DE-cadherin-mediated cell adhesion is essential for maintaining somatic stem cells in the *Drosophila* ovary. *Proc. Natl Acad. Sci. USA* **99,** 14813–14818 (2002).
24. Puch, S. *et al.* N-cadherin is developmentally regulated and functionally involved in early hematopoietic cell differentiation. *J. Cell Sci.* **114,** 1567–1577 (2001).
25. Schofield, R. The relathionship between the spleen colony-forming cell and the haematopoietic stem cell. A hypothesis. *Blood Cells* **4,** 7–25 (1978).
26. Dexter, T. M., Allen, T. D. & Lajtha, L. G. Conditions controlling the proliferation of haemopoietic stem cells *in vitro*. *J. Cell. Physiol.* **91,** 335–344 (1977).
27. Xie, T. & Spradling, A. C. A niche maintaining germ line stem cells in the *Drosophila* ovary. *Science* **290,** 328–330 (2000).
28. Calvi, L. M. *et al.* Osteoblastic cells regulate the haematopoietic stem cell niche. *Nature* **425,** 841–846 (2003).
29. Weissman, I. L. Developmental switches in the immune system. *Cell* **76,** 207–218 (1994).
30. Akashi, K. *et al.* Transcriptional accessibility for genes of multiple tissues and hematopoietic lineages is hierarchically controlled during early hematopoiesis. *Blood* **101,** 383–389 (2003).
31. Cheshier, S. H., Morrison, S. J., Liao, X. & Weissman, I. L. *In vivo* proliferation and cell cycle kinetics of long-term self-renewing hematopoietic stem cells. *Proc. Natl Acad. Sci. USA* **96,** 3120–3125 (1999).

Supplementary Information accompanies the paper on **www.nature.com/nature**.

Acknowledgements We thank P. Dijke for providing anti-BMPR1A anti-serum, and C. G. Lobe for Z/EG reporter mice. We thank R. Krumlauf and X. Liao for scientific discussion. We thank H. Lin for critically reviewing the manuscript, and L. Bonewald for training in bone histomorphometry. We are grateful to D. di Natale and T. Langner for assistance in manuscript editing. We are grateful to S. Morris and D. Stark for imaging assistance, W. Walker and her co-workers for animal care, and C. Sonnenbrot and his co-workers for assistance in medium preparation. This work was supported by the Stowers Institute for Medical Research.

Competing interests statement The authors declare that they have no competing financial interests.

Correspondence and requests for materials should be addressed to L.L. (lil@stowers-institute.org).

Osteoblastic cells regulate the haematopoietic stem cell niche

L. M. Calvi[1]*, G. B. Adams[3]*, K. W. Weibrecht[3], J. M. Weber[1], D. P. Olson[3], M. C. Knight[4], R. P. Martin[3], E. Schipani[4], P. Divieti[4], F. R. Bringhurst[4], L. A. Milner[2], H. M. Kronenberg[4] & D. T. Scadden[3]

[1]*Endocrine Unit, Department of Medicine, and* [2]*Department of Pediatrics, Center for Human Genetics and Molecular Pediatric Disease, University of Rochester School of Medicine, Rochester, New York 14642, USA*
[3]*Center for Regenerative Medicine and Technology, Partners AIDS Research Center, MGH Cancer Center, and* [4]*Endocrine Unit, Massachusetts General Hospital, Harvard Medical School, Boston 02114, Massachusetts, USA*

* These authors contributed equally to this work

Stem cell fate is influenced by specialized microenvironments that remain poorly defined in mammals[1–3]. To explore the possibility that haematopoietic stem cells derive regulatory information from bone, accounting for the localization of haematopoiesis in bone marrow, we assessed mice that were genetically altered to produce osteoblast-specific, activated PTH/PTHrP receptors (PPRs)[4]. Here we show that PPR-stimulated osteoblastic cells that are increased in number produce high levels of the Notch ligand jagged 1 and support an increase in the number of haematopoietic stem cells with evidence of Notch1 activation *in vivo*. Furthermore, ligand-dependent activation of PPR with parathyroid hormone (PTH) increased the number of osteoblasts in stromal cultures, and augmented *ex vivo* primitive haematopoietic cell growth that was abrogated by γ-secretase inhibition of Notch activation. An increase in the number of stem cells was observed in wild-type animals after PTH injection, and survival after bone marrow transplantation was markedly improved. Therefore, osteoblastic cells are a regulatory component of the haematopoietic stem cell niche *in vivo* that influences stem cell function through Notch activation. Niche constituent cells or signalling pathways provide pharmacological targets with therapeutic potential for stem-cell-based therapies.

Mammalian bone marrow architecture involves haematopoietic stem cells (HSCs) in close proximity to the endosteal surfaces[5,6], with more differentiated cells arranged in a loosely graduated fashion as the central longitudinal axis of the bone is approached[5,7,8]. This nonrandom organization of the marrow suggests a possible relationship between HSCs and osteoblasts—osteogenic cells lining the endosteal surface. Osteoblasts produce haematopoietic growth factors[9–11] and are activated by parathyroid hormone (PTH) or the locally produced PTH-related protein (PTHrP), through the PTH/PTHrP receptor (PPR). We tested whether osteoblasts contribute to the unique microenvironment of the bone marrow *in vivo* using a constitutively active PPR (col1-caPPR) under the control of the